Nano Energy 59 (2019) 574–581

Contents lists available at ScienceDirect

Nano Energy

journal homepage: www.elsevier.com/locate/nanoen

Full paper

Rich lamellar crystal baklava-structured PZT/PVDF piezoelectric sensor toward individual table tennis training

Guo Tian[a], Weili Deng[a,*], Yuyu Gao[a], Da Xiong[a], Cheng Yan[a], Xuebing He[a], Tao Yang[a], Long Jin[a], Xiang Chu[a], Haitao Zhang[a], Wei Yan[b], Weiqing Yang[a,*]

[a] *Key Laboratory of Advanced Technologies of Materials (Ministry of Education), School of Materials Science and Engineering, State Key Laboratory of Traction Power, Southwest Jiaotong University, Chengdu, 610031, PR China*

[b] *State Key Laboratory of Optical Technologies for Microfabrication, Institute of Optics and Electronics, Chinese Academy of Sciences, Chengdu, 610209, PR China*

A R T I C L E I N F O

Keywords:
Piezocomposite
PZT/PVDF
Lamellar crystal
Pressure sensor
Sports monitoring

A B S T R A C T

Real-time monitoring of interaction between ball and racket can provide the extremely important information for high quality guidance of individual table tennis training. However, the existing visual monitoring system is hard to reflect the specific interaction force and accurate hit position. Here, we design a self-powered rich lamellar crystal baklava-structured PZT/PVDF piezoelectric sensor for real-time monitoring of table tennis training and the scalable sports. This unique baklava-structured piezocomposite could be massively manufactured by a facile two step method of nonsolvent induced phase separation and hot-press process. As a result, the as-developed sensor exhibits preeminent sensitivity (6.38 mV/N) and ultrafast response time (21 ms). On this basis, we made a smart table tennis racket embedded with 6 × 6 units, which could real-timely fetch the hit location and contact force, then it could provide evaluation and individual guidance for the athletes training. Admittedly, this work not only opens a new way for real-time monitoring of impact location and force in table tennis training beyond current visual detection system, but also paves a new prospect for artificial intelligence electronics toward smart sports.

1. Introduction

Artificial intelligence (AI) facilitating our life has become more and more important in the society [1]. As an important part of AI, the intelligent sensor, making sports training more scientific and efficient through recording and analyzing the exercise data, is playing an increasingly crucial role in modern sports. Especially for racquet sports such as table tennis, the accurate hit location and quantitative contact force on the racket are the most critical indicators to assess the quality of shots and further scheme individual training plan. Unfortunately, the existing visual monitoring systems, such as the eagle eye in tennis tournament and the video assistant referee in football game, can just detect the trajectory of objects or the athletes posture but hardly fetch the specific interaction information between moving objects. In addition, costly equipment and massive data processing make it hard to realize real-time monitoring, especially for the high frequency interaction between the ball and racket. Hence, it is necessary and urgent to realize accurate and fast measurement of contact information.

The aforementioned functions could be achieved by pressure sensors based on diverse physical transduction mechanisms, including piezoresistive [2,3], capacitive [4,5], triboelectric [6–9] and piezoelectric sensor [10]. Among them, the piezoresistive and capacitive sensors are in favor of static measurements [11,12], which will intrinsically bring inconvenience to detect the high-frequency shock caused by the ball. Though the triboelectric sensor could measure the dynamic pressure [13–18], its contact-separation working mode is inherently not conducive to the movement of the ball [19,20]. In order to precisely detect the shots location and force, the piezoelectric sensor would be the ideal candidate due to its self-powered ability [21,22], high sensitivity [23] and fast response [24].

In this regard, numerous efforts have been paid to develop pressure sensor with different piezoelectric materials [25–29]. Compared with the traditional inorganic piezoceramics like ZnO [30], barium titanate (BTO) [31,32] and lead zirconate titanate (PZT) [33–36], or the organic piezoelectric polymer represented by polyvinylidene fluoride (PVDF) and its copolymer [37–40], the piezocomposite is more popular in recent years for possessing excellent piezoelectric and mechanical properties at the same time [41–45]. Among different composite patterns, the 0–3 composite has attracted great attention due to its facile fabrication and brilliant stability [46–48]. However, the lower energy

* Corresponding authors.
E-mail addresses: weili1812@swjtu.edu.cn (W. Deng), wqyang@swjtu.edu.cn (W. Yang).

https://doi.org/10.1016/j.nanoen.2019.03.013
Received 8 February 2019; Received in revised form 1 March 2019; Accepted 3 March 2019
Available online 06 March 2019
2211-2855/ © 2019 Published by Elsevier Ltd.

conversion efficiency of rough 0–3 composites badly limits its further commercial application. Hence, how to improve the piezoelectric properties of piezocomposites by intrinsically structured design is still a challenge at present.

Herein, we presented a facile two step method of nonsolvent induced phase separation and hot-press process to prepare rich lamellar crystal baklava-structured PZT/PVDF composites. This unique structure can helpfully disperse stress and thus has a faster response to identify each table tennis hit. Meanwhile, it effectively enhances the piezoelectricity due to the potential accumulation effect among each lamellar crystal and the synergistic effect formed by inorganic particles. Consequently, this fabricated piezocomposite exhibits glorious piezoelectricity even with relatively low doping content. Based on it, the as-fabricated piezoelectric sensor presented the open-circuit voltage (V_{oc}) of up to 2.51 V, short-circuit current (I_{sc}) as high as 78.43 nA and ultrafast response time of 21 ms. Integrated with 6 × 6 units, a smart table tennis racket was fabricated to real-timely detect the accurate hit location and precise impact force during training. Moreover, combined with communication module, a self-powered wireless real-time monitoring system has been successfully demonstrated. This work is expected to provide better individual training guidance for table tennis players through the data recorded by the designed sensors. More importantly, it paves a completely new idea for intelligent sensor toward smart sports beyond current visual system.

2. Results and discussion

2.1. Structured design of smart racket

As schematically shown in Fig. 1a, the smart racket consists of three parts: PZT/PVDF composites, signal processor and wireless transmitter module. In detail, the sensor array fabricated by PZT/PVDF composites is evenly distributed on the racket, meanwhile signal processor and wireless transmitter module are fixed on the racket handle. Furthermore, the detailed design of the device unit is schematically presented in Fig. 1b, which is a typical layered sandwich structure prepared through a convenient process. Here, the rich lamellar crystal baklava-structured piezocomposite acts as the functional layer, then the aluminum foils and Kapton films serve as electrodes and encapsulation severally. In this device, the layered baklava structure is in favor of stress release and thus could quickly response to external forces. Meanwhile, it has better stability because the layered structure can effectively avoid the damage of the whole structure. In addition, the potential accumulation of different lamellar crystal makes it more sensitive to pressure. Accordingly, to obtain such baklava-structured piezoelectric material, we adopted a facile two step method of nonsolvent induced phase separation combined with hot-press process, where the schematic process was illustrated in Fig. 1c and the fabrication details were further described in Experimental Section. Furthermore, a sensor array is integrated on the racket to detect the signal of table tennis as elucidated in Fig. 1d, then the hit location and contact force could be quantitatively obtained, it is expected to provide individual training guidance for players.

2.2. Fabrication and characterization of the piezocomposite

In order to get better piezoelectricity, several efforts have been devoted to increase the content of β-phase crystal in PVDF. Its molecule configuration, as shown in Fig. 2a, has strong polarity owing to its all-trans conformation [49,50]. However, the poor conductivity of PVDF is inconvenient to the transmission of charges, hence it is difficult to enhance piezoelectric property just through intrinsic polymer modification. In fact, the inorganic particles usually serve as the synergetic phase to improve the piezoelectricity of piezocomposites, but the performance improvement depends largely on the composite structure, where the fabrication process plays a decisive role. In this work, the delicate process concept is presented in Fig. 2b. Firstly, the composite manufactured by the method of nonsolvent induce phase separation has tangled structure as depicted in Fig. 2b **i**, which takes advantage of the different solubilities of water to the N, N-dimethylformamide (DMF) and PVDF (Experimental details are illustrated in Fig. S1). Due to the extremely rapid phase separation process, this method allows the PZT particles dispersed evenly in the PVDF matrix compared to traditional solvent-casting and drying, which tends to cause the aggregation of inorganic particles during the relatively long drying process [51]. Subsequently, the sample is heated and once the temperature excesses the glass transition temperature of PVDF, the tangled molecule chain will disentangle and the local order chain will form as displayed in Fig. 2b **ii**. At the same time, the inorganic PZT particles will serve as nucleus and thus the polymer chains assemble around it to crystallize, which contributes to the improvement of crystallinity. Finally, the ultra-high pressure is applied to transform the conformation of PVDF chain to obtain all-trans conformation β-phase lamellar crystals, and the inorganic particles are implanted in lamellar crystal to enhance piezoelectricity (Fig. 2b **iii**).

Based on the above conception, the perovskite structured PZT particles were chose to prepare the piezocomposite with different weight contents from 0 to 33.33% through the two step method. (Its detailed

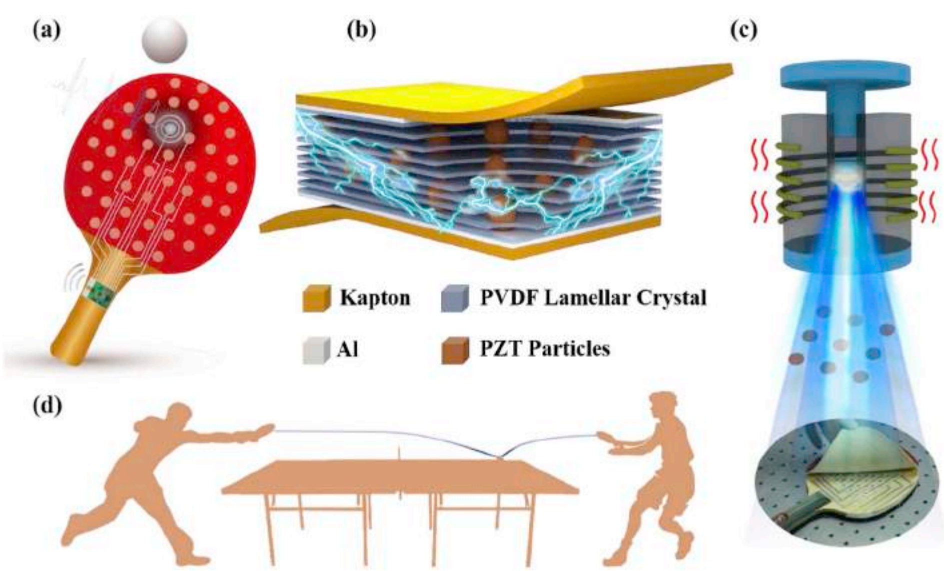

Fig. 1. Schematic illustration of the smart training system. (a) Schematic illustration of the smart racket for table tennis monitoring. (b) The general illustration and detailed structure of the designed sensor. (c) The fabrication process of the piezocomposite and optical photograph of the smart racket. (d) The application of the smart table tennis racket.

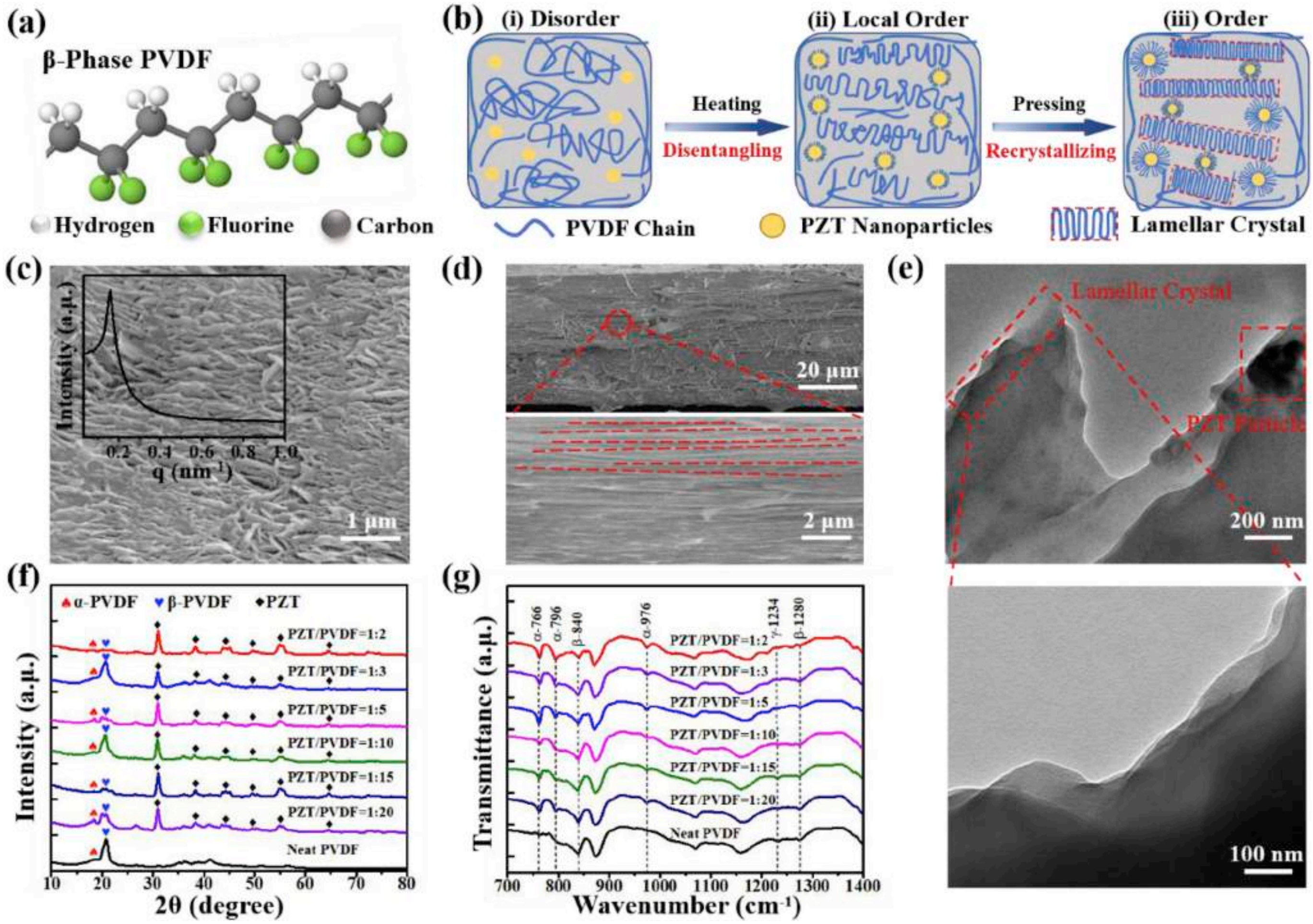

Fig. 2. Structure design and characterization of the piezocomposite. (a) The molecular structure of β-phase PVDF. (b) The conception of preparing β-phase lamellar crystal. (c) The surface SEM image of the sample, the inset shows the SAXS result. (d) The cross-sectional SEM images of the fabricated piezocomposite. (e) The TEM images of the sample. (f) FTIR and (g) XRD results of the PZT/PVDF composite with distinct compound ratios.

structure and morphology are presented in Fig. S2 [33].) The layered lamellar crystal structure of sample is distinctly observed by scanning electron microscope (SEM) as displayed in Fig. 2c, and the inset is the result of small-angle X-ray scattering (SAXS), where the intense scattering peak (0.16 nm^{-1}) proves the existence of long period layered lamellar crystal in the sample, and the distance among different lamellar crystal is about 36.25 nm, which is ideally consistent with the SEM results [52]. Likewise, the special layered structure is observed from the cross-sectional SEM image of the composite (Fig. 2d), and the thickness is about 80 μm, which ensures the flexibility of the sample. Furthermore, the transmission electron microscope (TEM) is applied to verify the composite structure, the layered lamellar crystal embedded with PZT particles is clearly observed as shown in Fig. 2e and the enlarged view. All these characteristics indicate the rationality of the design concept. In addition, the X-ray diffraction (XRD) and Fourier Transform Infrared Spectroscopy (FTIR) are further used to characterize the phase structure of the composite. From the XRD pattern (Fig. 2f), it is obvious that the diffraction peak intensity varies with the doping concentration, the peak of 30.99° indicating the (101) crystal face of PZT and the peak of 20.26° indicating the β-phase of PVDF reach a relatively large value simultaneously when the doping ratio is 1:10, which means the better piezoelectricity than neat PVDF and better flexibility than PZT. Besides, as displayed in Fig. 2g, the results of FTIR demonstrate that doping will change the crystal behavior and then regulate the content of β-phase in the composite. The peak at 840 cm^{-1} tickets the existence of β-phase, and the α-phase peak assigns at 766 cm^{-1}, then the β-phase content can be obtained as shown in Table S1 [53]. From the results, it can be found that the content of β-phase shows a fluctuation with the diverse doping concentration and the peak value occurs when the PZT doping weight ratio reaches 1:10, these results are in good agreement with the result of XRD. Its possible reason is that there are two antagonistic effects generated by PZT particles in the composite. On the one hand, the PZT particles will damage the regularity of the macromolecule chain, which is opposite to the crystallization. On the other hand, some PZT particles with suitable size will serve as the nucleus to increase crystallinity at the same time. In our experiment, these two effects reach a balance when the composite weight ratio is 1:10, and massive layered lamellar β-phase crystals are obtained as displayed in Fig. 2e.

To further investigate the performance of the fabricated piezocomposite, the electrical performances are measured under different vertical pressures, and the whole measure system is presented in Fig. S3. The working principle of the piezoelectric composite is schematically shown in Fig. 3a. As depicted in this figure, the piezoelectricity contains the output of β-phase lamellar crystal and the synergistic effect induced by the PZT particles. For the former, the electron clouds are asymmetrically distributed on both sides of the molecule chain, which comes from the different ability of groups to attract electrons as shown on the left of Fig. 3a. When the pressure is exerted, the deformation of molecule chain leads to the disruption of electron cloud equilibrium state. To resume the balanced state, the electrons will flow through the chain to form piezopotential. More importantly, the layered lamellar crystal structure tends to produce larger deformation than other crystal structure under vertical pressure, thus the layered lamellar crystal structure will generate stronger

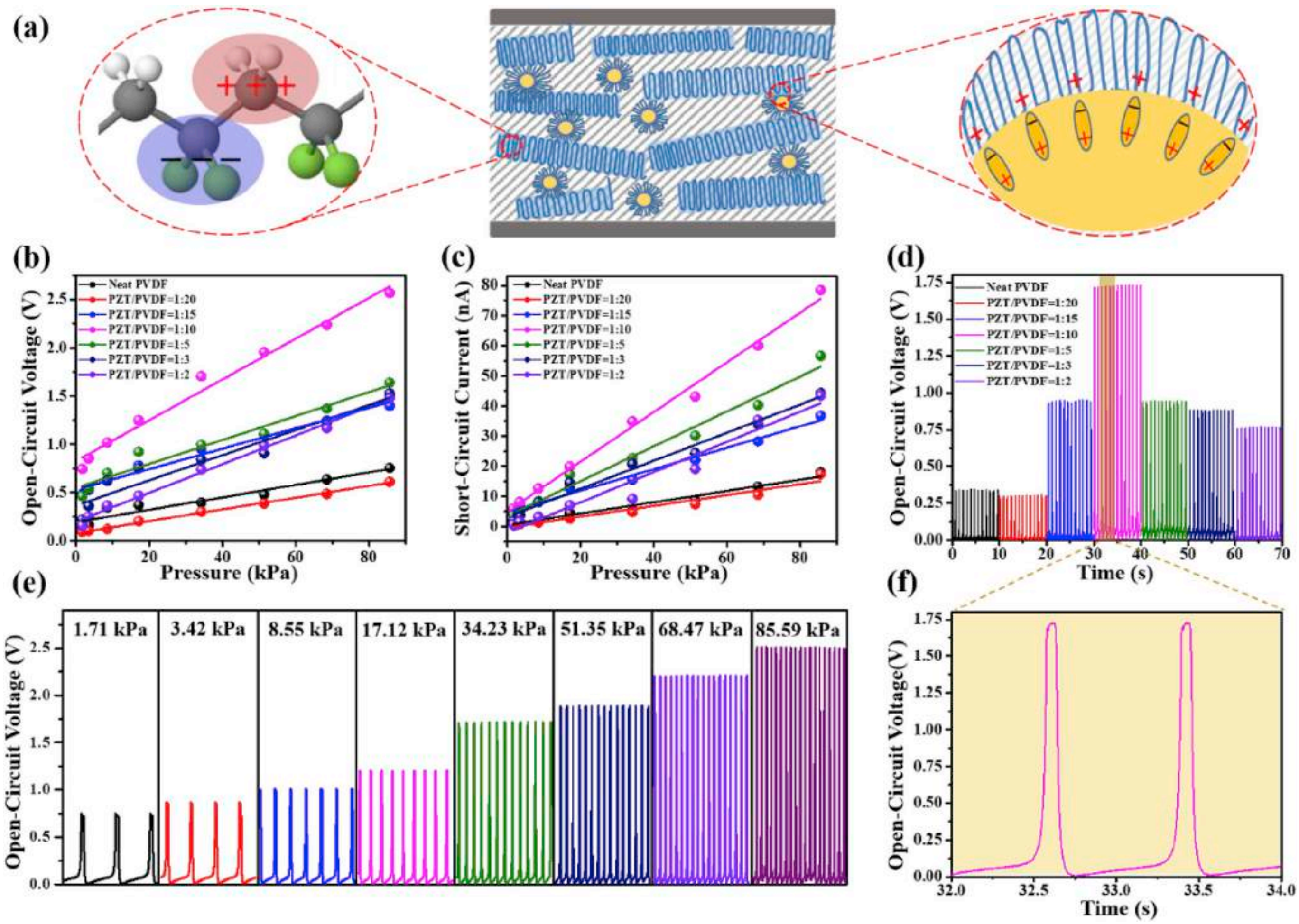

Fig. 3. Electromechanical measurement of the device. (a) Schematic diagram of the distribution of piezoelectric charges. (b) V_{oc} and (c) I_{sc} of the composite with different weight ratios on a range of increasingly pressures. (d) The V_{oc} varies with diverse PZT particles content from 0 to 33.33% under 34.23 kPa. (e) V_{oc} of the sensor with a weight ratio of 1:10 under different pressures. (f) Enlarged view of the V_{oc} in two strike periods.

piezopotential. Another contribution of output originates from the synergistic effect induced by PZT particles. In the layered lamellar crystal structure, the charges generated by PVDF will interact with the PZT particles as shown on the right of Fig. 3a. Through accumulation effect, the potential could accumulate layer by layer with the help of the embedded PZT particles, which could be regarded as the channel of potential accumulation in the composite. Therefore, the doping of inorganic particles is conducive to improving piezoelectricity of composites. However, through increasing the doping content, the piezopotential promotion is usually accompanied by the decline in flexibility, as a result, there will be a balance state between doping content and properties.

In order to investigate the relationship between doping content and electrical performance of the device, the relative electrical measurements were further carried out, and the results of V_{oc} and I_{sc} were presented in Fig. 3b and c respectively. Obviously, the output varying with the doping content and the variational tendency faultlessly agree with the above structure characterization of the composite. Among different doping ratios, the composite obtains the best electrical performance when the doping ratio reaches 1:10. This phenomenon could be attributed not only to the abundant content of PZT particles, but also the high content of β-phase lamellar crystal in this sample. Moreover, the electrical outputs present well linearity proving the excellent performance of the device as pressure sensor. Besides, the tendency of output varying with the doping content is further analyzed under the external pressure of 34.23 kPa, as shown in Figs. 3d and S4. It can be found that the maximum output could respectively achieve up to 1.71 V and 34.83 nA when the weight ratio is 1:10. And from the magnified two-cycle V_{oc} signal displayed in Fig. 3f, the device exhibits quick response under external pressure. This property reveals the immense potential for measuring the dynamic forces. Besides, the detailed results about the output voltage varying with the doping content are clearly illustrated in Fig. S5. Evidently, when the doping ratio is 1:20, it is too low to induce phase transition in the sample, the nucleation induced by PZT particles is less than the destruction of molecular chains thus the β-phase content is declining than neat PVDF. Although the β-phase content decreased, the synergistic output generated by the inorganic particles would make up the output. Hence, there is no distinct decrease in output than the neat PVDF. Later, with the increase of doping content, the synergistic effect and the content of β-phase lamellar crystal are raised synchronously, which promotes the sharp increase of V_{oc}. When the doping ratio reaches 1:10, the best performance is obtained. After that, the V_{oc} begins to decline when the content of PZT particles exceeds the critical point. The possible reason is that the redundant PZT particles prevent the orderly alignment of molecular chain, which destroys the formation of β-phase lamellar crystal structure. This result conforms perfectly to the original hypothesis of the working principle, and the devices prepared by the presented method possess excellent piezoelectricity even under the low doping content. Among different external pressures, the electrical outputs of the device with weight ratio of 1:10 are shown in Figs. 3e and S6. It can be seen from the picture that the piezocomposite shows superior electrical performance reaching up to 2.51 V and 78.43 nA under 85.59 kPa, and has good mechanical stability in a wide pressure range, which attributes to the distinctive structure in the sample.

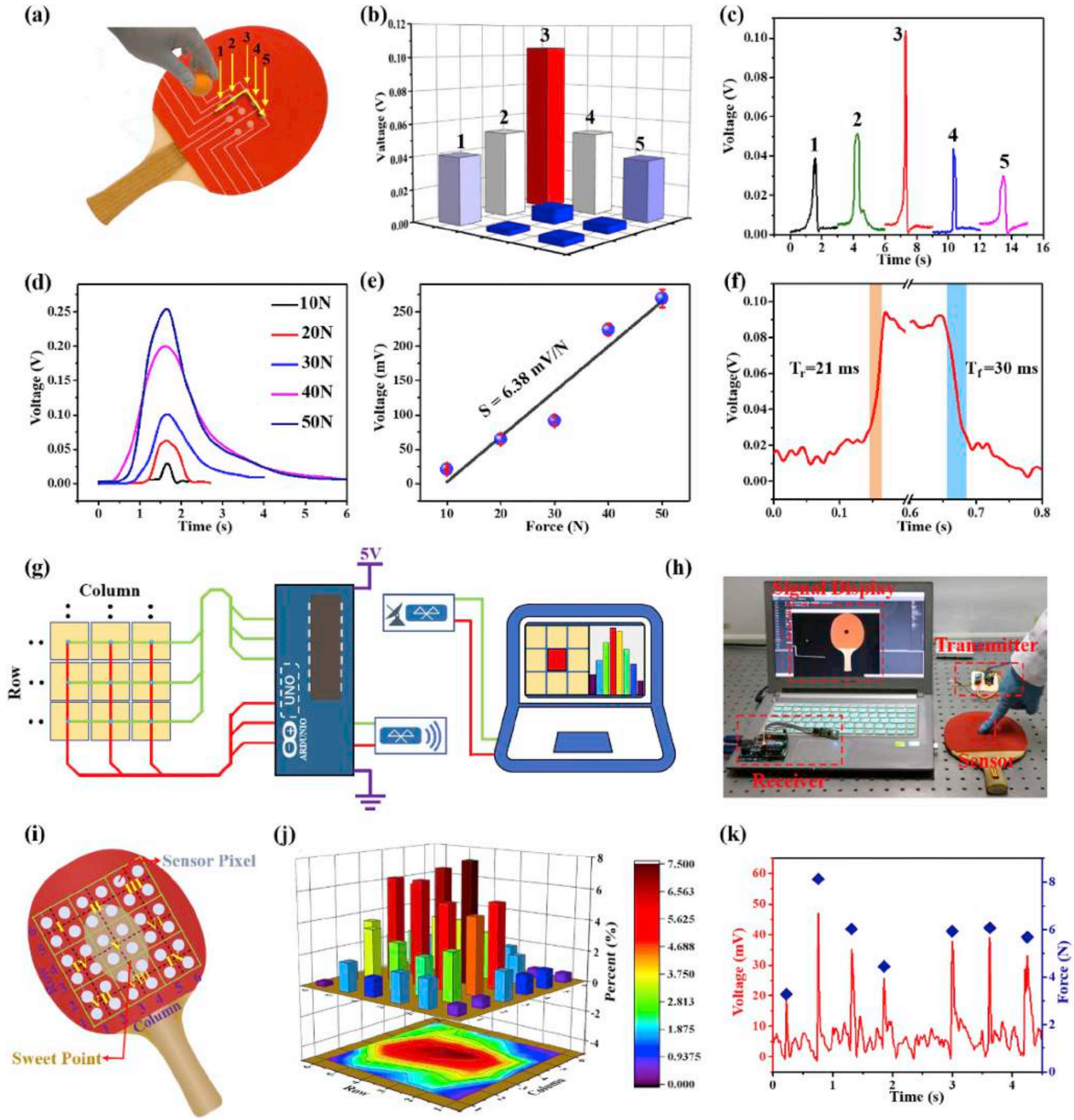

Fig. 4. Application of the smart racket. (a) Schematic illustrations of a ball moving along a path. (b) and (c) The corresponding voltage output of the sensor when the ball moving along the path. (d) The V_{oc} under various forces on the racket. (e) The pressure sensitivity of the sensor, the error bars result from multi-measurement. (f) Response time of the sensor. (g) The working principle of the wireless detecting system. (h) The photograph of wireless system presenting the function of locating the ball. (i) The distribution of the sensor pixel and sweet point on the racket. (j) Bar charts showing the statistic distribution percent of hits. (k) The voltage output and the force for a series of shots.

2.3. The application of the smart racket

Based on its preeminent performance, we further verified the application of the piezocomposite sensor toward individual table tennis training. For proving the potential to detect hit location, a 3 × 3 units with the cross-type electrodes are integrated on the racket as shown in Fig. 4a, and a ball held by hand moves along a Γ-path on the sensor array. The corresponding results are shown in Fig. 4b and c, which indicate that the motion path of the ball could be clearly recorded, even the motion speed could be estimated from the electrical response. Meanwhile, this measurement demonstrates that there is no serial interference amongst different sensing pixel. On this basis, the sensor array could be applied to path tracking, motion speed calculating and other applications. It should be emphasized that another indispensable factor to evaluate the shot quality is the hit strength. However, the current visual monitoring system could hardly achieve this purpose. To scale the hit strength accurately and reduce the disturbance for player, the as-developed sensor is implanted into the rubber sheet in practical measure, and the further result is shown in Fig. 4d. Obviously, the response magnitudes of the fabricated sensor increase with forces even if most of the force is absorbed by the rubber sheet, which owes to the excellent pressure sensitivity of layered lamellar crystal and thus shows great potential for practical application. After the output is measured five times under every set force, the average values are recorded in Fig. 4e, which displays splendid stability with the pressure. Furthermore, the pressure sensitivity (ΔV/ΔF, where ΔV is the difference of output voltage and ΔF is the difference of exerted force) of the fabricated sensor could reach up to 6.38 mV/N through the linear fitting of these data, which exhibits the commendable ability to scale the hit force. At the same time, for recording the real-time signal, another key indicator is the response time, which must be less than the interval of contiguous two shots in actual training. From Fig. 4f, it can be seen that the response time, defined as the time of the response signal rising/falling from 10% to 90%, are 21 ms and 30 ms respectively, which is about twice as fast as the neat PVDF device (55 ms) [54]. This ultrafast response owes to the rapid stress release originated from the layered lamellar crystal structure, because there is plenty gap between the different lamellar crystals to release stress, it is in favor of achieving real-time monitoring for each shot.

Furthermore, in order to apply the developed sensor in actual training, the system is ineluctably designed to be wireless [55], which is schematically elucidated in Fig. 4g. Here, the sensors are integrated into the racket to measure the signals of dynamic hit process, when the ball hits on the racket, the electric signal generated by the sensor is collected by an Arduino board, then these data will be sent to the computer via a Bluetooth module. Furthermore, to analyze these data timely, the visual window is constructed by Python in the computer, where the data could be observed in time [56]. The optical photograph of the wireless sensing system is presented in Fig. 4h, which consists of the sensor, the transmitter, the receiver and the computer. When the ball or finger acts on the sensor, the detailed interaction information will be accurately measured and wirelessly transmitted to the computer, further there will be a legible signal and the color of the sensor will change on the displayer (The related video is shown in Supporting Information Movie S1). Afterwards, the signals of dynamic hit process were further measured, which verified the possibility of applying the smart table tennis racket in actual training (The related video could be found in Supporting Information Movie S2). As can be seen, the as-developed sensor could accurately detect the hit position and force, meanwhile the specific information could be real-timely displayed in the forms of pictures and numerical values.

Supplementary data related to this article can be found at https://doi.org/10.1016/j.nanoen.2019.03.013.

In addition, another important index called sweet point is applied for appraising the hit quality in practical training. When the ball hits on the sweet point, the ball will get a faster velocity and less swing, hence, locating the area for each shot is significant for guiding players. The distribution of sweet point on the racket is shown in Fig. 4i and the 6 × 6 sensing units evenly distributed on the racket are used to locate the hit point and scale the contact force. In this experiment, about 20000 times hits were applied for collecting credible data. As a result, the statistical probability for every pixel hit is presented in Fig. 4j and the sums of probability for different areas are recorded in Fig. S7. From the statistic results, it is easy to find out the distribution of shot points, which could be used to evaluate the shot quality. Furthermore, the specific voltage output and contact force could be quantitatively recorded simultaneously, and the results of one unit within a few shots are displayed in Fig. 4k. Combined the above information, the interaction between ball and racket could be analyzed in detail, then the quality of the shot would be fully reflected. In the training, the coach could keep abreast of the player state and customize individual training plan. Beyond that, the fabricated sensor could also be used in table tennis robot. On account of the excellent performance of the fabricated sensor, the robot could calculate the flight path of the ball through the recorded data, and adjust execution command in response. The designed smart table tennis racket introduces an innovative way to locate the hit point and contact force, which can quickly couple back the signal to the processor and actuator. This is of great significance to promote the development of intelligent robot.

3. Conclusion

In conclusion, we developed a self-powered rich lamellar crystal baklava-structured PZT/PVDF piezoelectric sensor for high quality guidance of individual table tennis training. Through a facile two step method, the as-prepared piezocomposite exhibits eximious electrical performance in virtue of the potential accumulation effect and the synergistic effect even with relatively low doping ratio of 1:10. Further, V_{oc} and I_{sc} of the PZT/PVDF based device could reach up to 2.51 V and 78.43 nA, respectively. More importantly, the sensor, fabricated by the as-developed layered lamellar crystal composite, displays a list of amazing features, such as high sensitivity of 6.38 mV/N, fast response time of less than 21 ms and excellent stability. On this basis, we developed a smart table tennis racket embedded with 6 × 6 sensing units, which could real-timely fetch the hit location and contact force, beneficially evaluate the competitive state and scientifically scheme individual training guidance for players. Unambiguously, this smart racket affords a novel application for sensor in smart sport monitoring beyond current visual assistant system, and is expected to bring a revolution in intelligent sensors.

4. Experimental section

4.1. Preparation of the piezocomposite

The PVDF (Kynar PVDF 761A, Arkema) and the PZT particles (QiJin New Materials Co., Ltd) were dispersed in DMF respectively, then the former stirred for 3 h at 70 °C and the other stirred for 3 h at indoor temperature. When the PVDF dissolved and the PZT particles dispersed in the DMF, mixed the two solutions together and continue to stir for 5 h. On this basis, the mixed solution was dropped into the deionized water, the PVDF with PZT particles dispersed would deposit and the DMF would be dissolved in water. Later, the composite was going to be dried at 80 °C for 12 h and be cut into pieces. In order to get preeminent piezoelectricity, the composite was put into a home-made piston-cylinder as shown in Fig. 1c, and heating it to 200 °C for 10 min to melt. Then a pressure of 150 MPa was applied and temperature was elevated to 260 °C for reconstructing the PVDF chain. After the target temperature was reached, the pressure was further raised to 400 MPa for 10 min to form the layered β-phase lamella crystal. Finally, quench down to ambient conditions with the pressure and the sample was obtained. The prepared sample has a thickness about 80 μm and diameter of 8 mm.

4.2. Fabrication of the device

The sensor was fabricated briefly. First, the samples were adhered with aluminum foil on both sides as electrodes, then copper wire was used to draw electrodes. Next, the array was encapsulated by Kapton film. Finally, the whole device was implanted into the rubber sheet, the smart racket was fabricated.

4.3. Characterization and measurements

The SEM and TEM images were gained from JEOL JSM7800F Prime and JEOL JEM-2100F respectively. The SAXS was performed by Xeuss 2.0 (France, Xenocs) and Pilatus 3 detector, the radiation wavelength is about to 0.154 nm. XRD patterns were got with a DX-1000 diffractometer. FTIR result was obtained by a Nicolet 5700 spectrometer ranging from 700 to 4000 cm^{-1}. The electric measurement system was shown in Fig. S4, a NTIAG HS01–37 × 166 linear motor was applied as the external stimulate. The electrical performance of the sample was measured by Keithley 6514 and a low-noise current preamplifier (Stanford Research SR570). The wireless signal acquisition system was composed of two Arduino boards and two Bluetooth 4.0 modules.

Notes

The authors declare no competing financial interest.

Acknowledgments

The authors thank for the support from the National Natural Science Foundation of China (No. 61801403), the Scientific and Technological Projects for International Cooperation of Sichuan Province (No. 2017HH0069), the Fundamental Research Funds for the Central Universities of China (No. 2682017CX071), and the Independent Research Project of State Key Laboratory of Traction Power (No. 2017TPL_Z04). Appreciate the help from the Analysis and Testing Center of Southwest Jiaotong University.

Appendix A. Supplementary data

Supplementary data to this article can be found online at https://doi.org/10.1016/j.nanoen.2019.03.013.

References

[1] M.L. Jordan, T.M. Mitchell, Science 349 (2015) 255–260.
[2] M. Jian, K. Xia, Q. Wang, Z. Yin, H. Wang, C. Wang, H. Xie, M. Zhang, Y. Zhang, Adv. Funct. Mater. 27 (2017) 1606066.
[3] Y.N. Ma, N.S. Liu, L.Y. Li, X.K. Hu, Z.G. Zou, J.B. Wang, S.J. Luo, Y.H. Gao, Nat. Commun. 8 (2017) 1207.
[4] Y. Zang, F. Zhang, D. Huang, X. Gao, C.A. Di, D. Zhu, Nat. Commun. 6 (2015) 6269.
[5] H.K. Lee, J. Seo, S. Shin, J.H. Koo, C. Pan, S. Son, J.H. Kim, Y.H. Jang, D.E. Kim, T. Lee, Adv. Mater. 27 (2015) 2433–2439.
[6] B.B. Zhang, L. Zhang, W.L. Deng, L. Jin, F.J. Chun, H. Pan, B.N. Gu, H.T. Zhang, Z.K. Lv, W.Q. Yang, Z.L. Wang, ACS Nano 11 (2017) 7440–7447.
[7] Y. Yang, Y.S. Zhou, H.L. Zhang, Y. Liu, S. Lee, Z.L. Wang, Adv. Mater. 25 (2013) 6594–6601.
[8] Z.L. Wang, J. Chen, L. Lin, Energy Environ. Sci. 8 (2015) 2250–2282.
[9] N.N. Zhang, C. Tao, X. Fan, J. Chen, J. Mater. Res. 32 (2017) 1628–1646.
[10] Q.Z. Zhong, J.W. Zhong, X.F. Cheng, X. Yao, B. Wang, W.B. Li, N. Wu, K. Liu, B. Hu, J. Zhou, Adv. Mater. 27 (2015) 7130–7136.
[11] Z. Lou, S. Chen, L. Wang, K. Jiang, G.Z. Shen, Nanomater. Energy 23 (2016) 7–14.
[12] S. Gong, W. Schwalb, Y. Wang, Y. Chen, Y. Tang, J. Si, B. Shirinzadeh, W. Cheng, Nat. Commun. 5 (2014) 3132.
[13] P. Bai, G. Zhu, Q. Jing, J. Yang, J. Chen, Y. Su, J. Ma, G. Zhang, Z.L. Wang, Adv. Funct. Mater. 24 (2014) 5807–5813.
[14] C. Wu, W. Ding, R. Liu, J. Wang, A.C. Wang, J. Wang, S. Li, Y. Zi, Z.L. Wang, Mater. Today 21 (2018) 216–222.
[15] R. Cao, X. Pu, X. Du, W. Yang, J. Wang, H. Guo, S. Zhao, Z. Yuan, C. Zhang, C. Li, Z.L. Wang, ACS Nano 12 (2018) 5190–5197.
[16] X.D. Wang, Y.F. Zhang, X.J. Zhang, Z.H. Huo, X.Y. Li, M.L. Que, Z.C. Peng, H. Wang, C.F. Pan, Adv. Mater. 30 (2018) 1706738.
[17] Z.M. Lin, J. Chen, X. Li, Z. Zhou, K. Meng, W. Wei, J. Yang, Z.L. Wang, ACS Nano 11 (2017) 8830–8837.
[18] Z. Lin, J. Yang, X. Li, Y. Wu, W. Wei, J. Liu, J. Chen, J. Yang, Adv. Funct. Mater. 28 (2018) 1704112.
[19] J. Chen, Z.L. Wang, Joule 1 (2017) 480–521.
[20] J. Yang, J. Chen, Y. Su, Q. Jing, Z. Li, F. Yi, X. Wen, Z. Wang, Z.L. Wang, Adv. Mater. 27 (2015) 1316–1326.
[21] F.R. Fan, W. Tang, Z.L. Wang, Adv. Mater. 28 (2016) 4283–4305.
[22] K.W. Zhang, S.H. Wang, Y. Yang, Adv. Energy Mater. 7 (2017) 1601852.
[23] B. Wang, C. Liu, Y. Xiao, J. Zhong, W. Li, Y. Cheng, B. Hu, L. Huang, J. Zhou, Nanomater. Energy 32 (2017) 42–49.
[24] J. Zhou, P. Fei, Y.F. Gao, Y.D. Gu, J. Liu, G. Bao, Z.L. Wang, Nano Lett. 8 (2008) 2725–2730.
[25] D.Y. Park, D.J. Joe, D.H. Kim, H. Park, J.H. Han, C.K. Jeong, H. Park, J.G. Park, B. Joung, K.J. Lee, Adv. Mater. 29 (2017) 1702308.
[26] L. Jin, S.Y. Ma, W.L. Deng, C. Yan, T. Yang, X. Chu, G. Tian, D. Xiong, J. Lu, W.Q. Yang, Nanomater. Energy 50 (2018) 632–638.
[27] N. Wu, X. Cheng, Q. Zhong, J. Zhong, W. Li, B. Wang, B. Hu, J. Zhou, Adv. Funct. Mater. 25 (2015) 4788–4794.
[28] D.B. Deutz, N.T. Mascarenhas, J.B.J. Schelen, D.M. Leeuw, S. Zwaag, P. Groen, Adv. Funct. Mater. 27 (2017) 1700728.
[29] C. Dagdeviren, P. Joe, O.L. Tuzman, K.I. Park, K.J. Lee, Y. Shi, Y.G. Huang, J.A. Rogers, Extre. Mech. Lett. 9 (2016) 269–281.
[30] Y. Yang, W.X. Guo, Y. Zhang, Y. Ding, X. Wang, Z.L. Wang, Nano Lett. 11 (2011) 4812–4817.
[31] K.I. Park, S. Xu, Y. Liu, G.T. Hwang, S.J. Kang, Z.L. Wang, K.J. Lee, Nano Lett. 10 (2010) 4939-4343.
[32] Y. Kim, K.Y. Lee, S.K. Hwang, C. Park, S.W. Kim, J. Cho, Adv. Funct. Mater. 24 (2014) 6262–6269.
[33] C. Dagdeviren, Y. Su, P. Joe, R. Yona, Y. Liu, Y.S. Kim, Y. Huang, A.R. Damadoran, J. Xia, L.W. Martin, Y.G. Huang, J.A. Rogers, Nat. Commun. 5 (2014) 4496.
[34] Z. Chen, Z. Wang, X. Li, Y. Lin, N. Luo, M. Long, N. Zhao, J.B. Xu, ACS Nano 11 (2017) 4507–4513.
[35] K.I. Park, C.K. Jeong, J. Ryu, G.T. Hwang, K.J. Lee, Adv. Energy Mater. 3 (2013) 1539–1544.
[36] C. Yan, W.L. Deng, L. Jin, T. Yang, Z. Wang, X. Chu, H. Su, J. Chen, W.Q. Yang, ACS Appl. Mater. Interfaces 10 (2018) 41070–41075.
[37] X. Han, X. Chen, X. Tang, Y.L. Chen, J.H. Liu, Q.D. Shen, Adv. Funct. Mater. 26 (2016) 3640–3648.
[38] X. Chen, H. Tian, X. Li, J. Shao, Y. Ding, N. An, Y. Zhou, Nanoscale 7 (2015) 11536–11544.
[39] S.N. Cha, S.M. Kim, H.J. Kim, J.Y. Ku, J.I. Sohn, Y.J. Park, B.G. Song, M.H. Jung, E.K. Lee, B.L. Choi, J.J. Park, Z.L. Wang, J.M. Kim, K. Kim, Nano Lett. 11 (2011) 5142–5147.
[40] C. Ribeiro, C.M. Costa, D.M. Correia, J.N. Pereira, J. Oliveira, P. Martins, R. Goncalves, V.F. Cardoso, S.L. Mendez, Nat. Protoc. 13 (2018) 681–704.
[41] C. Zhang, Y. Fan, H. Li, Y. Li, L. Zhang, S. Cao, S. Kuang, Y. Zhao, A. Chen, G. Zhu, Z.L. Wang, ACS Nano 12 (2018) 4803–4811.
[42] N.R. Alluri, B. Saravanakumar, S.J. Kim, ACS Appl. Mater. Interfaces 7 (2015) 9831–9840.
[43] R. Ding, X.L. Zhang, G. Chen, H.L. Wang, R. Kishor, J.X. Xiao, F. Gao, K.Y. Zeng, X.D. Chen, X.W. Sun, Y.J. Zheng, Nanomater. Energy 37 (2017) 126–135.
[44] C.K. Jeong, J. Lee, S. Han, J. Ryu, G.T. Hwang, D.Y. Park, J.H. Park, S.S. Lee, M. Byun, S.H. Ko, K.J. Lee, Adv. Mater. 27 (2015) 2866–2875.
[45] W.L. Deng, T. Yang, L. Jin, C. Yan, H.C. Huang, X. Chu, Z.X. Wang, D. Xiong, G. Tian, Y.Y. Gao, H.T. Zhang, W.Q. Yang, Nanomater. Energy 55 (2019) 516–523.
[46] E.J. Lee, T.Y. Kim, S.W. Kim, S. Jeong, Y. Choi, S.Y. Lee, Energy Environ. Sci. 11 (2018) 1425–1430.
[47] K.I. Park, M. Lee, Y. Liu, S. Moon, G.T. Hwang, G. Zhu, J.E. Kim, S.O. Kim, D.K. Kim, Z.L. Wang, K.J. Lee, Adv. Mater. 24 (2012) 2999–3004.
[48] Q.B. Zhai, Y. Yang, Adv. Mater. Technol. 2 (2017) 1700161.
[49] Y.Y. Choi, P. Sharma, C. Phatak, D.J. Gosztola, Y.Y. Liu, J. Lee, B. Lee, J.Y. Li, A. Gruverman, S. Ducharme, S. Hong, ACS Nano 9 (2015) 1809–1819.
[50] Prateek, V.K. Thakur, R.K. Gupta, Chem. Rev. 116 (2016) 4260–4317.
[51] J.I. Kim, Y. Choi, K.Y. Chung, J.H. Park, Adv. Funct. Mater. 27 (2017) 1701768.
[52] Y. Li, S. Tang, M.W. Pan, L. Zhu, G.J. Zhong, Z.M. Li, Macromolecules 48 (2015) 8565–8573.
[53] P. Martins, A.C. Lopes, S.L. Mendez, Prog. Polym. Sci. 39 (2014) 683–706.
[54] C.R. Deng, W. Tang, L. Liu, B. Chen, M.C. Li, Z.L. Wang, Adv. Funct. Mater. 28 (2018) 1801606.
[55] S.H. Wang, X.J. Mu, Y. Yang, C.L. Sun, A.Y.D. Gu, Z.L. Wang, Adv. Mater. 27 (2015) 240–248.
[56] K. Zhao, Z.L. Wang, Y. Yang, ACS Nano 10 (2016) 9044–9052.

Guo Tian received his B.E. degree in Material Science and Engineering from Southwest Jiaotong University (SWJTU), PR China in 2018. He is currently pursuing master's degree at SWJTU. His research interest includes piezoelectric materials and functional devices.

Weili Deng received his M.E. degree from Chongqing University in 2009, and Ph.D. in Materials Science and Engineering from Southwest Jiaotong University in 2016. He was a teacher at Southwest Jiaotong University from 2009. His main research interest includes sensor and flexible electronics, such as piezoelectric sensor and photoelectric detection.

Yuyu Gao received his B.E. degree in Materials Science and Engineering from Southwest Jiaotong University, PR China in 2018. He is now a mastercandidate in Material Science and Engineering at SWJTU. His research interest includes sensitive materials and functional devices.

Long Jin received his B.E. from Southwest Jiaotong University in 2015. He is currently pursuing Ph.D. degree in materials science and engineering at Southwest Jiaotong University.

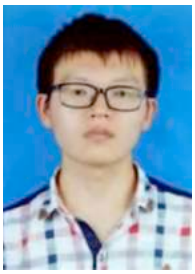

Da Xiong received his B.E. degree in Materials Science and Engineering from Southwest Jiaotong University in 2018. Now he is a master candidate in Materials Science and Engineering at Southwest Jiaotong University. His recent research focuses on flexible optoelectronic devices and sensors.

Xiang Chu received his B.E. degree in Materials Science and Engineering from Southwest Jiaotong University (SWJTU), PR China in 2016. He is now a doctoral candidate in Materials Science and Engineering at SWJTU. His research interest includes nano-materials for electrochemical energy storage devices.

Cheng Yan received his B.E. from Southwest Jiaotong University in 2017. He is currently pursuing Ph.D. degree in materials science and engineering at Southwest Jiaotong University. His research focuses on the flexible electronics and self-powered sensors.

Haitao Zhang received his Ph.D degree in Electrical Engineering from Institute of Electrical Engineering in 2015, Chinese Academy of Sciences. He is now an Asistant Prof. in Southwest Jiaotong University (Chengdu, China). His main research interest focus on new energy materials and their electrochemical energy storage devices including supercapacitors, Li—S batteries, and CO_2 batteries.

Xuebing He received his B.E. degree in Materials Science and Engineering from Southwest Jiaotong University (SWJTU), PR China in 2016. Now, he is master candidate a in Materials Science and Engineering at SWJTU. His research focuses on polymer processing.

Wei Yan is a professor in State Key Laboratory of Optical Technologies for Microfabrication, Institute of Optics and Electronics, Chinese Academy of Sciences. His main research interest focus on the development of microelectronic equipment and related key technologies of micro-nano optics and optical measurement.

Tao Yang received his B.E. in materials science and engineering from Southwest Jiaotong University in 2017. He is currently pursuing master's degree in materials science and engineering at Southwest Jiaotong University. His research focuses on the flexible electronics and self-powered sensors.

Weiqing Yang received his M.S. in Physics in 2007, and Ph.D. in Materials Science and Engineering from Sichuan University in 2011. He was a post-doctorate research fellow at University of Electronic Science and Technology of China from 2011 to 2013. Subsequently, he was a post-doctorate research fellow at Georgia Institute of Technology from 2013 to 2014, under the supervision of Prof. Zhong Lin Wang. His main research interest includes energy harvesting and storage devices, such as supercapacitors and nanogenerators.